Ultrahigh Specific Power Electrochemistry, Exemplified by Al/MnO_4^- and Cd/AgO Redox Chemistry

Stuart Licht*

Department of Chemistry, Technion, Israel Institute of Technology, Haifa, 32000 Israel

Noseung Myung

Department of Applied Chemistry, Kon-Kuk University Chungju Campus, Chungju, Chungbuk 380-701 Korea

Dharmasena Peramupage

EIC Corporation, Norwood, Massachusetts

Received: February 6, 1998

An unusual charge transfer domain for electrochemical processes is investigated. Criteria are described which facilitate an ultrahigh specific power domain. This domain is defined for faradaic processes that are long when compared to the electrochemical double layer charging time, as a specific power over 10000 W/kg occurring at a specific energy over 1 Wh/kg. Traditionally compared to capacitors, faradaic processes can achieve high specific energy, >1 Wh/kg, but limited specific power, <1000 W/kg. Experimental evidence and examples of irreversible and quasi-reversible processes which occur in the ultrahigh power domain are presented. Each has a specific power approaching one million W/kg. The irreversible example establishes electrochemical control of the chemically reactive couple: $Al + MnO_4^- + 2H_2O \rightarrow Al(OH)_4^- + MnO_2$, $E_{cell} = 2.9$ V. The quasi-reversible (secondary) example utilizes a conventional macroscopic silver/cadmium couple systematically reduced to the submicron and micron microelectrochemical cross section domain (submicron Ag and Cd electrodes separated by a 5 μm interelectrode gap).

Introduction

There have been few experimental explorations into the fundamental electrochemical constraints of the highest specific power domain. The highest limiting rates of charge transfer for electrochemical storage processes have not been clearly delineated despite the need for higher power electrochemical storage in consumer electronics, electrical vehicle, and peak power reserve applications. Conventional storage redox couples provide a relatively high energy capacity (high specific energy), but low specific power. The kinetics and configuration of typical devices such as batteries and fuel cells limits their specific power to significantly less than 1000 W/kg. Despite this limitation, the predominance of research on the electrochemistry of storage processes has focused on increasing electrochemical specific energy; conventional redox couples provide specific energy of 20−300 W h/kg, with improvements studied.[1−4] Existing specific power limitations has led to exploration of capacitor and hybrids using both faradaic and capacitive processes for applications including mobile communications, miniature and pulsed lasers, terrestrial, nautic, aeronautic, and aerospace electric vehicles.[1,5−6] In this study we describe both irreversible and quasi-reversible examples of faradaic process with specific power approaching a MW/kg over a discharge time that is long when compared to capacitive double layer times (≫1 ms).

This study explores criteria for an electrochemical power domain which approaches the capacitor specific power domain. In their simplest mode, capacitors store energy via electrostatic processes, as opposed to faradaic processes requiring (oxidative/reductive) charge transfer. Capacitors are capable of delivering energy quickly (high specific power), but store less energy than faradaic devices. A class of devices that have capacitor-like discharge characteristics, but have a specific energy which approaches that found in the faradaic domain, have been termed as "pseudocapacitors", "ultracapacitors", or "supercapacitors".[6] These are based on either double layer or absorbed monolayer phenomena or on metal oxides, or on conductive polymers with reported specific energies of up to 10 Wh/kg. Of these, high surface area carbon ultracapacitors have the highest specific power approaching 10^4 W/kg. This is exemplified by a aerogel carbon electrochemical double layer capacitor with a specific power of 7500 W/kg.[7]

In capacitors or supercapacitor devices the variation of current approximates a rectangular response to the linear modulation of potential with time.[6] For a device of capacitance, C (in farads), the current density, is given by $C\mathrm{d}V/\mathrm{d}t$. The time dependence t of an initial potential V_o (volts), through a load resistance, $R(\Omega)$, is $V_o e^{-t/RC}$ and therefore the power density P through a surface area, $A(\mathrm{cm}^2)$, is given by

$$P(\mathrm{W/cm}^2) = V_o^2/ARe^{-2t/RC} \quad (1)$$

Alternately, electrochemical faradaic processes, with the reversible cell potential given by the difference of the anode and cathode redox potentials, $V_o = E_{cathode} - E_{anode}$, exhibit a high degree of irreversibility, with overpotential increasing with increasing current density. When current I (amps) flows through the electrode, the cell power is diminished due to electrode activation and concentration overpotentials, η_{act} and η_{conc}, and also due to ohmic loss in the cell, principally localized in the resistive electrolyte $R_{electrolyte}$. The cell power is given by

$$P(\mathrm{W/cm}^2) = (V_o - (\eta_{cathode,act} + \eta_{anode,act}) - (\eta_{cathode,conc} + \eta_{anode,\,conc}) - IR_{electrolyte})^2/A \quad (2)$$

In either faradaic or capacitive power density, specific power

S1089-5647(98)01048-7 CCC: $15.00
Published on Web 08/11/1998

is enhanced by minimization of the area normalized, total mass of the cell components

$$m_{\text{total}}\ (\text{kg/cm}^2) = A(\text{cm}^2)^{-1}\Sigma_i m_i\ (\text{kg}) \qquad (3)$$

yielding a specific power, P_s:

$$P_s(\text{W/kg}) = P(\text{W/cm}^2)/m_{\text{total}}\ (\text{kg/cm}^2) \qquad (4)$$

An unusually high specific power domain for faradaic processes is investigated. Criteria are described which facilitate the ultrahigh power domain, which is defined as a specific power over 10000 W/kg occurring at specific energy over 1 Wh/kg, for faradaic discharge times which are long when compared to the electrochemical double layer charging time.

Experimental Section

Materials. Silver and cadmium electrodes were either "thin" (Sigma) 25 μm thick Ag or Cd planar sheet or "ultrathin". Ultrathin cadmium electrodes are 0.25 μm electrodeposited Cd on an 0.076 μm Au leaf (VWR). Cd (0.25 μm, 0.22 mg/cm^2) was deposited from 0.25 *m* $CdCl_2$, 2.7 *m* NaCN, 0.5 *m* NaOH for 7 min at 0.89 mA/cm^2. Analytical grade reagents and distilled, deionized water were used throughout. Ultrathin silver electrodes are 0.10 μm Ag leaf (VWR). Nickel cathodes for permanganate reduction consist of either planar Ni or highly porous nickel 100 ppi, pore per inch (Eltec RETEC Ni). Aluminum anodes were either Alcan International 99.999% Al or Alcan International DH50V Al alloy containing >99% Al alloyed with Mg, Sn, and Ga.

Instrumentation and Measurement Techniques. Cadmium and silver cyclic voltammetry was measured using a conventional three electrode potentiostatic configuration with a PINE RDE5 potentiostat, including an Ag/AgCl reference, and the indicated working electrode separated by 0.2 cm from a large Pt mesh counter electrode. Electrochemistry of the silver/cadmium ultrahigh power domain was investigated using a cell comprised of electrodes, staged between the 0.2 cm^2 circular plates of a Stanley Micrometer vernier caliper (with 1 μm flatness and readout to 10 μm precision). Sodium carboxymethylcellulose (1%) was added to the (9 *m* NaOH) cell electrolyte, increasing solution viscosity and preventing electrolyte leakage. Cell current was measured at applied cell potentials with a PINE RDE5 potentiostat using a two electrode configuration (shoted reference and counter electrode). The applied cell potential was generated with a Heath R74 sweep function generator applying a square wave to the potentiostat potential input. In the cell, interelectrode separation was systematically reduced using several spacers and separators including: 750 μm neoprene (McMaster), 50 μm Teflon (McMaster), 12.5 μm solid Teflon film (Goodfellow), and 80% porous 12.5 μm Teflon film (Goodfellow), and the thinnest cell employed a washer cut from 5 μm solid Teflon film (Goodfellow) as a spacer.

Galvanostatic measurements for oxidation of aluminum or reduction of permanganate were performed in the aforementioned conventional three electrode configuration without IR compensation, although in a highly conductive electrolyte (100 °C, 3 *m* KOH aqueous electrolyte), and therefore provide an upper bound to the electrode overpotential η. The aluminum coulombic utilization measurements were performed with a constant load cell, to full consumption of the Al anode, and efficiency determined by comparing the coulombs generated during Al oxidation to the theoretical 3 e^- faradaic equivalents

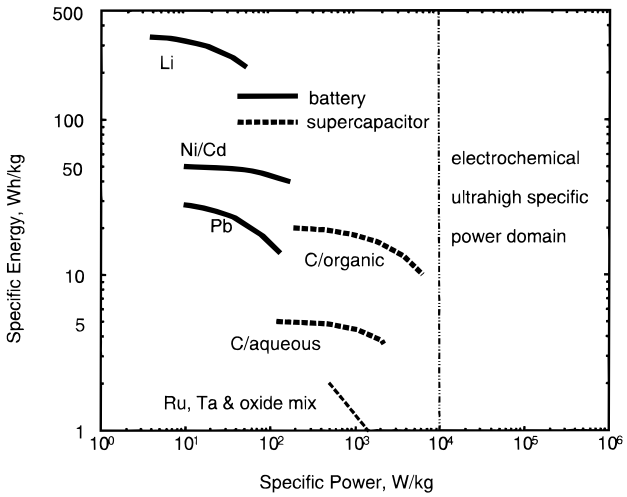

Figure 1. Specific power versus specific energy plot for faradaic and supercapacitor devices. The ultrahigh electrochemical power domain is indicated on the right portion of the figure. Battery and supercapacitor data is modified from ref 1.

available in the mass of the exposed, consumed anode. Cell potential and current were measured with GW MACDIOS8 data acquisition. Coulombs generated were verified on a EG&G PAR 379 digital coulometer.

In the aluminum/permanganate ultrahigh power investigations, planar aluminum and nickel electrodes were separated by a 30 μm Teflon spacer. The electrolyte is maintained in an 0.042 cm diameter capillary and injected by pressurized argon into the aluminum/nickel electrode cell; cell and capillary were maintained at a constant temperature (100($\pm$0.3) °C) in a thermostatic bath. Injection of the permanganate electrolyte into the cell triggered discharge and initiated a 2.5 kHz digitized voltage acquisition (by Zenith SD5000 digital storage oscilloscope).

Results and Discussion

Ultrahigh Electrochemical Power Domain. We define the electrochemical ultrahigh specific power P_s domain to consist of specific powers of over 10000W/kg at a discharge time, t_d, which is long when compared to capacitive electrochemical double layer times $\gg$1 ms), and yielding a specific energy density, E_s, of over 1 Wh/kg:

$$E_s = P_s t_d > 1\ \text{Wh/kg} \qquad (5)$$

Figure 1 compares the specific power and specific energy and several conventional faradaic and supercapacitor devices. The right-hand portion of the figure sets minima to an alternate domain and delineates a region of specific power which is substantially higher than that of conventional faradaic processes and is also a region of specific energy higher than that of capacitors. This right-hand portion represents the ultrahigh electrochemical power domain.

Criteria For Ultrahigh Power. For faradaic processes limited to low current densities *J*, power losses generally occur due to a lack of electrocatalysis (activation overpotential). At moderate *J*, the electrolyte resistance also contributes to the power loss, but at the highest current densities mass transport limitations may also lead to power shutdown. In eq 2, the activation overpotential, concentration overpotential, and electrolyte resistance are dependent variables. Hence, $R_{\text{electrolyte}}$ will tend to diminish as the electrolyte concentration is increased up to several molar. Similarly, although the activation overpotential is often evaluated under conditions of excess redox

constituents, it varies strongly at high current density conditions, due to the concentration depletion which will occur at the electrode surface. In accord with conventional Butler−Volmer theory for an n electron transfer, the activation overpotential η_{act} dependence on the current density, is given by

$$J = J_o[\exp(\alpha n_a F\eta_{act}/RT) - \exp(-(1-\alpha)nF\eta_{act}/RT)] \quad (6)$$

where α is the transfer coefficient, and J_o is the exchange current density. Equation 6 at high current density simplifies to (using $b = 1/\alpha n$ or $b = 1/(1 - \alpha n)$ respectively, for anodic or cathodic reactions) an expression for current density which increases with temperature:

$$J(\mathrm{A/cm^2}) = -J_o(\mathrm{A/cm^2})\exp(\eta F/bRT) \quad (7)$$

Faradaic exchange currents vary considerably (from J_o less than 1 pA/cm^2 to J_o over 1 A/cm^2). Hence, under appropriate nonmass transport limited, nonelectrolyte resistance limited conditions, systems with a large J_o can generate current densities in the domain of A/cm^2. Equations 2−4 and 6−7 establish several clear criteria for high power: (1) kinetically facile anodic and cathodic redox couples; (2) a high activity of redox constituents relative to electrode surface area; (3) a low electrolyte resistance; (4) time domains longer than the double layer time, but short compared to the onset of mass transport limitations, and discharge time t_d on the order of milliseconds to seconds for concentrated aqueous cells; finally, (5) a low cross sectional thickness of each of the cell components compared to its mass m_i.

High Power Microelectrochemical Domain. In this study, two experimental studies of the criteria of the ultrahigh power domain are probed, each establishes faradaic processes than can have specific power approaching 1 MW/kg. The first example utilizes criteria 3−5 and maximization of power via eqs 3−5, to derive a microelectrochemical ultrahigh power extrapolation of an existing quasireversible (secondary) electrochemical storage couple. This is accomplished by reducing utilization of a silver/cadmium redox couple to the micron and submicron domain. The second strategy focuses on criteria 1 and 2 and presents primary ultrahigh power electrochemistry on the basis of energetic redox couples (aluminum in a permanganate medium) not usually associated with electrochemical storage.

Microelectrochemistry has focused on the minimization of electrode surface area, resulting in enhanced diffusion and low double layer charging curents, and minimization of $R_{electrolyte}$ interference, thereby permitting effects such as ultrafast voltammetry,[8] studies of resistive media,[8] and the discrimination of a small number of redox active species.[9] The microelectrochemistry of a cell cross section is an additional important domain to be considered, and this spatial domain will have significant power and energy ramifications. For example, investigators, such as Buck et al., have looked at fundamental of thin layer electrochemical cells,[10] and thin layer (10−20 μm) polymer electrolyte cells have been studied, although it should be noted that such systems will lead to high specific energy, but not high specific power, due to the very high relative resistance of such systems compared to aqueous medium.

In accord with eq 4, as the thickness of a planar electrode of fixed surface area is reduced to the submicron level, when the total redox charge transferred through the electrode is retained, the effective specific power increases proportionally with the reduction in cross section. The upper portion of Figure 2 presents the conventional cyclic voltammetry of planar cadmium and silver electrodes at 75 °C in alkaline media, and in each

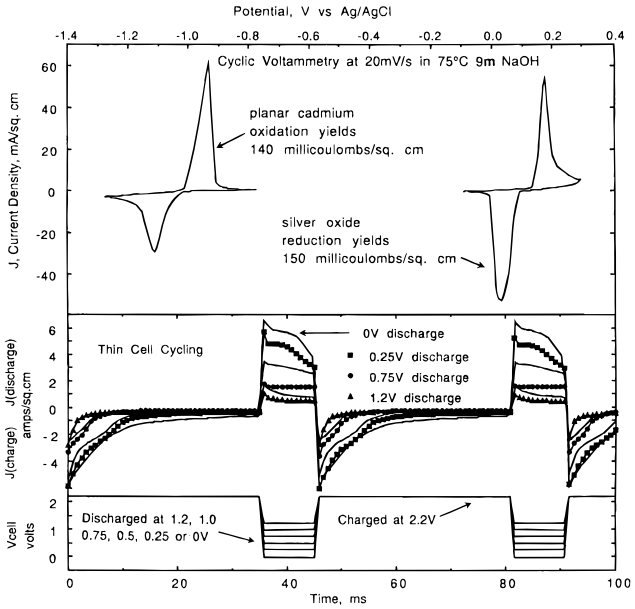

Figure 2. Top: Cyclic voltammetry of planar cadmium or planar silver in a 9 *m* NaOH solution at 75 °C and a sweep rate of 20 mV/s. Bottom: 75 °C rapid repeated discharge behavior of a thin silver/cadmium cell discharged for 10 ms at various discharge potentials. Cell comprised of 25 μm thick Ag and Cd electrodes, separated by 9 *m*, NaOH, 1% cellulose electrolyte with a 750 μm neoprene spacer.

case integration yields 140−150 mcoulombs/cm^2 per cycle on these planar electrodes. The theoretical one electron capacity of 0.15 μm thick silver is equivalent to 141 mcoulombs/cm^2. In the absence of surface modification, this total charge is independent of the cross sectional dimensions down to these submicrom dimensions. As the cross section thickness of the electrodes is reduced to this domain, the sustainable charge transferred becomes a larger fraction of the theoretical charge capacity of the electrodes. The lower portion of Figure 2 includes charge/discharge behavior of a relatively thin (25 μm Ag and Cd electrodes separated by a 750 μm spacer) secondary silver/cadmium cell:

$$Cd + Ag_2O \rightarrow CdO + 2Ag \quad E_{cell} = 1.2\ V \quad (8)$$

As seen in the figure, for repeated 10 ms discharges, discharges of 0.5 to over 5 A/cm^2 can be sustained at 75 °C. The cell maximum power point occurs at 0.5−0.75 *V*. Note that the generated charge of 5−50 mcoulomb/cm^2 is clearly faradaic. This charge is larger than that attributable to monolayer adsorption of ∼0.1 mcoulomb/cm^2 and occurs at times which are long when compared to the concentrated aqueous double layer discharge time of less than 1 ms.

The first of the ultrahigh power domain strategies minimizes $A/\Sigma m_i$, eq 3, by the stepwise reduction in silver/cadmium cell cross section toward the high specific power domain. The first reduction of interelectrode separation from 750 down to 50 μm required the addition of a porous separator and diminishes the 0.75 V discharge current density from $J = 1.5$ down to 1.0 A/cm^2, respectively presented as open circles and solid triangles in Figure 3. Use of the thinnest commercially available porous separator available, an 80% porous 12.5 μm Teflon separator, further restricts current flow resulting in $J = 0.8$ A/cm^2, indicated by the solid circles within the figure. As an alternative to the spacer we have added 5 μm SiO_2 particles to the electrolyte (10% by weight) which effectuates electrode autonomy across a 5 μm interelectrode cross section. Finally, the 25 μm thick electrodes are replaced with 0.1 μm Ag and 0.25

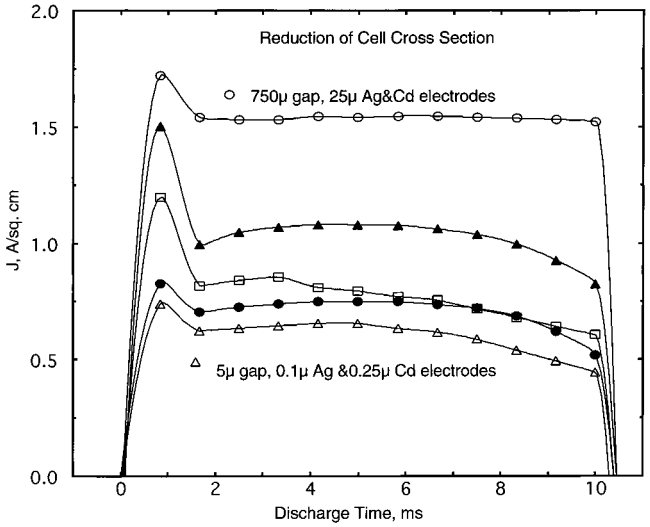

Figure 3. Constant potential (0.75 V), rapid (10 ms) discharge behavior of several silver/cadmium cell configurations at 75 °C. Cell configurations: open circles, cell containing a 750 μm interelectrode gap. Solid triangles, with a 50 μm interelectrode gap and containing a porous separator. Open squares, with a 50 μm interelectrode gap and containing no separator, but the electrolyte contains 10% by mass of 5 μm particles of SiO_2. Solid circles, with a 12.5 μm interelectrode gap and containing a porous separator. Open triangles, with a 5 μm interelectrode gap and containing no separator, but the electrolyte contains 10% by mass of 5 μm particles of SiO_2. 5 and 12.5 μm gap cells use submicron thick electrodes (0.1 μm Ag and 0.25 μm Cd). 50 and 750 μm gap cells utilize 25 μm thick Ag and Cd electrodes. Electrolyte is 9 *m* NaOH, 1% cellulose alone, or also containing 10% by weight 5 μm solid SiO_2 particles.

μm Cd electrodes. As seen by the open triangles in the figure, the combined effects of the 5 μm SiO_2 particles and the submicron metal electrodes still permit an 0.75 V discharge current density of $J = 0.5-0.75$ A/cm^2 for a power density of $\sim$0.5 W/cm^2. This power density is sustained with micron and submicron components composed of 5 μm thick electrolyte (9 *m* NaOH with 1% cellulose and 10% SiO_2) at 0.68 mg/cm^2, and electrode masses for the 0.25 μm Cd (0.22 mg/cm^2) on an 0.076 μm Au leaf of 0.15 mg/cm^2, and an 0.10 μm Ag leaf at 0.11 mg/cm^2. In accord with eq 4, the microelectrochemical cross section of the individual electrodes and the interelectrode gap yields a small mass per unit area and a high specific power. Combined these components yield a total mass, $\Sigma m_i = 1.16$ mg/cm^2. Hence, the 0.5 W/cm^2 generates a specific power of 430000 W/kg.

A representation of this microelectrochemical cross section cell is presented in the right portion of Figure 4. The cell exhibits 500000 reproductive charge/discharge cycles at 25 °C, but over this same period at 75 °C the current density, while higher for the first several thousand cycles, diminishes several fold, a fact we attribute to inadequate encapsulation and electrolyte loss over time. Discharge curves under a variety of discharge conditions are summarized in the left corner of the figure, with peak power densities of 0.5 MW/kg and a sustained specific power of 0.4 MW/kg being observed. The 10 ms discharge releases 6 mcoulomb/cm^2 and produces a specific energy of 1.1 Wh/kg. A longer duration (2500 millisecond) discharge releases 53 mcoulomb/cm^2, which is a significant fraction of the limiting faradaic capacity of the 0.1 μm Ag electrode and produces a specific energy of 10.7 Wh/kg.

Energetic Redox High Power Domain. In a second strategy, consistent with the first of the high power criteria, energetic, kinetically facile redox couples can be used to substantially enhance power. Electrode kinetics are limited by

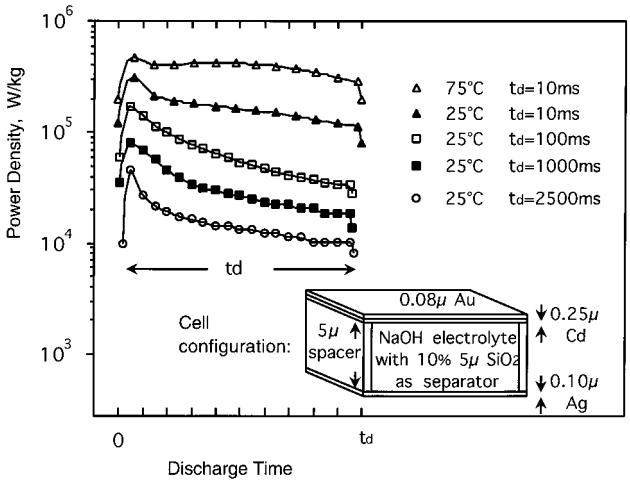

Figure 4. Secondary silver/cadmium ultrahigh power cell behavior for various repeated 0.75 V discharges. This cell, represented in the lower right of the figure, uses 0.25 μm thick Cd and 0.10 μm Ag separated by 5 μm. The 9 *m* NaOH, 1% cellulose (by weight) electrolyte contains 10% 5 μm solid SiO_2 particles (by weight) to prevent interelectrode contact.

the exchange current density exchange J_o, which at a low overpotential, η(V cm^2/A) is given for an *n* electron transfer by[10]

$$J_o = (\lim \eta \rightarrow 0)\, RT/\eta Fh = 0.0000862\ \mathrm{V}T(\mathrm{K})/n\eta \quad (9)$$

Measured values of J_o often strongly depend on surface and electrolyte preparation, and reported values vary widely in the literature.[11] For power evaluations, the highest sustainable current density and the polarization measured at a planar electrode provide a reproducible assessment of the steady state power. We observe that a 1 cm^2 planar aluminum anode in an alkaline permanganate electrolyte will support continuous planar current densities in the A/cm^2 domain, these current densities are 1−4 orders of magnitude higher than those observed for planar anodes of redox couples considered in conventional electrochemical storage processes.[3,12] In accord with eq 7, sustainable current densities and polarization losses decrease with increasing temperature. As presented in Figure 5, a planar aluminum anode in alkaline permanganate will sustain oxidation current density up to 2 A/cm^2, incurring maximum polarization losses of $\eta = 0.3$ V cm^2/A^{-1} at $T = 373$ K, and $\eta = 0.8$ V cm^2 A^{-1} at $T = 348$ K. These polarization losses do not include compensation for solution resistance and provide only an upper bound to η. The Tafel plot of log(current) versus this uncompensated overpotential attest to a large value of i_o, providing an extrapolated lower bound of the exchange current of $J_o > 1$A/cm^2.

Electronegative anodes such as aluminum might be considered incompatible (reactive) when immersed in a strong oxidizing agent such as aqueous permanganate. However, in principle these reactive systems present the energy differences which permit unusually high power densities to be extracted. We have recently demonstrated a model in which efficient electrochemical energy may be derived from aluminum in contact with strong chemically reactive oxidizers.[13−15] Due to passivation and blocked charge transfer, many anodic and cathodic electrochemical storage electrodes exhibit lower coulombic efficiencies at higher current densities. However, the opposite can occur for anodic aluminum in contact with reactive cathodic redox couples. In this case, using cathodes also capable of high current densities in alkaline media, upon rapid discharge the rate of

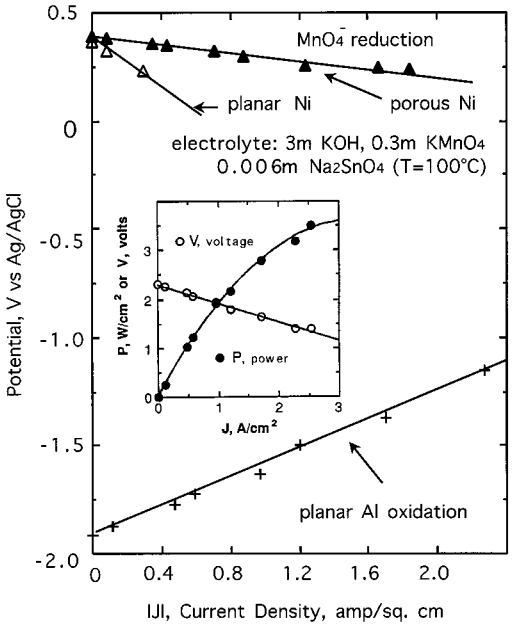

Figure 5. Current/voltage galvanostatic measurements for oxidation of aluminum or reduction of permanganate in 3 *m* KOH, 0.3 *m* $KMnO_4$, and 0.006 *m* Na_2SnO_4 electrolyte at 100 °C; Electrocatalytic cathodes for permanganate reduction were either planar Ni or exposed 100 ppi porous Ni. Absolute values of the oxidative or reductive current density *J* are shown. Inset: Polarization and power curves for 0.5 cm^2 aluminum/permanganate cells at 100 °C. Cells contained 0.5 cm^2 100 ppi porous Ni cathode (both sides exposed), spaced 0.2 cm from 0.5 cm^2 AB50V Al (one side exposed) and are immersed in stirred aqueous 3 *m* KOH, 0.3 *m* $KMnO_4$, 0.006 *m* Na_2SnO_3.

electrochemical charge transfer can dominate over parasitic chemical charge transfer reactions, permitting efficient electrochemical use of the stored energy. A ferricyanide cathode was previously utilized to demonstrate that such high coulombic efficiency aluminum electrochemical storage systems are possible; however, the cell had a modest specific energy limited by the high mass of ferricyanide salts.[14]

As seen in Figure 5, permanganate reduction currents approach 0.4 A/cm^2 on planar Ni (or Pt), at which point the cathode is observed to passivate with an MnO_2 overlayer. This is avoided by use of a highly porous Ni electrode which permits sustainable permanganate reduction currents also approaching 2A/cm^2 with low polarization losses of 0.1 V cm^2/A. At current densities above 2 A/cm^2, MnO_2 formation again passivates the electrodes. In this alkaline medium the permanganate reduction occurs in two separate steps ($MnO_4^- \rightarrow MnO_4^{2-} \rightarrow MnO_2$) and appears to be rate limited by the latter step to MnO_2. Whereas the one electron reduction to manganate is facile (as observed with the depletion of the 526 nm permanganate peak and with the simultaneous rise of the 602 nm manganate absorption peak) the subsequent two electron reduction from manganate to MnO_2 is slower resulting in the observed passivating layer at the highest current densities.

The individual aluminum anodic and permanganate cathodic redox half reactions may be summarized as

$$\text{anode:}\quad Al + 4OH^- \rightarrow Al(OH)_4^- + 3e^- \qquad E° = 2.3\ \text{V vs SHE} \quad (10)$$

$$\text{cathode:}\quad MnO_4^- + 2H_2O + 3e^- \rightarrow MnO_2 + 4OH^- \qquad E° = 0.6\ \text{V vs SHE} \quad (11)$$

for a highly energetic overall process:

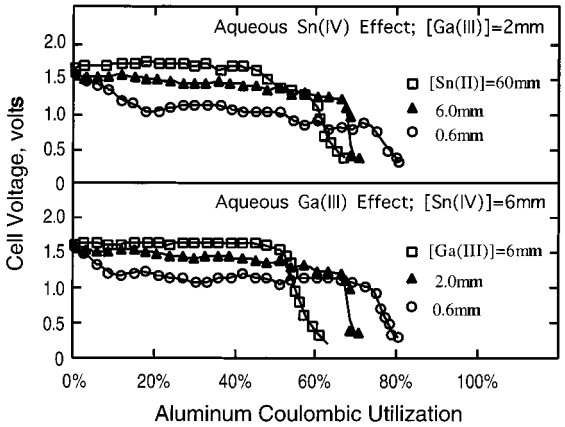

Figure 6. Cell voltage and coulombic efficiency of aluminum oxidation during discharge of aluminum/permanganate cells; effects are shown of solution phase additives. Anodes are composed of "pure" 99.999% Al. Discharges are over a 2.2 Ω load at 100 °C. Electrolyte is 3 *m* KOH, 0.3 *m* $KMnO_4$ with various concentrations of the indicated additives. Sn(IV) and Ga(III) refer to Na_2SnO_3 and Ga_2O_3 additives. Cells were discharged to full consumption of an 0.05 cm thick Al anode. Cells were configured with a two sided 0.5 cm^2 100 ppi porous Ni cathode, situated 0.2 cm from 0.5 cm^2 of the anode (one side exposed), and in alkaline permanganate electrolyte.

$$Al + MnO_4^- + 2H_2O \rightarrow Al(OH)_4^- + MnO_2 \qquad E_{cell} = 2.9\ \text{V} \quad (12)$$

When based on lithium, sodium, or potassium permanganate salts, this system is characterized by the high theoretical specific energies respectively of 1230, 1140, and 1070 Wh/kg.[16] The inset of Figure 5 presents current and power density versus cell voltage, for the measured aluminum/potassium permanganate cell at 100 °C. In accord with the separate anode and cathode measurements in the main portion of the figure, an open circuit potential in excess of 2 V is observed. High current densities are sustained by the system, including sustained power densities of 3.5 W/cm^2. At current densities above 2 A/cm^2, as well as in the absence of induced convention (rapid stirring), formation of a film of the product, MnO_2, is visible which passivates both electrodes.

Effective use of the first of the listed criteria for ultrahigh power requires control of active, energetic redox couples, and a variety of effects were studied to enhance the discharge potential and the efficient coulombic utilization of aluminum towards optimization of an aluminum/permanganate cell. The aluminum/permanganate cells are investigated by immersing parallel Al anodes and Ni electrocatalytic cathodes in aqueous permanganate solutions. Use of a large cathode surface area minimizes polarization losses and allows the study of anode and electrolyte effects. Aluminum oxidation can be substantially modified by solution phase additives,[13−21] and we observe related effects in permanganate electrolytes. As illustrated in Figure 6, at 100 °C, added Sn(IV) or Ga(III) oxides stabilize and increase the cell voltage permitting high aluminum discharge currents. However, high concentrations (60 m*m*, Sn(IV) or 6 m*m* Ga(III)) decrease the coulombic utilization of pure (99.999%) aluminum.

Alternatively, aluminum may also be activated by incorporation of metals directly (alloying) into the anode.[22−24] Figure 7 compares improved discharge characteristics with one such alloy (containing > 99% Al and < 1% Mg, Sn and Ga) to the pure aluminum anode. The alloy aluminum discharge exhibits improved voltage characteristics while retaining high anodic utilization efficiencies. In accord with our model system,[13,14]

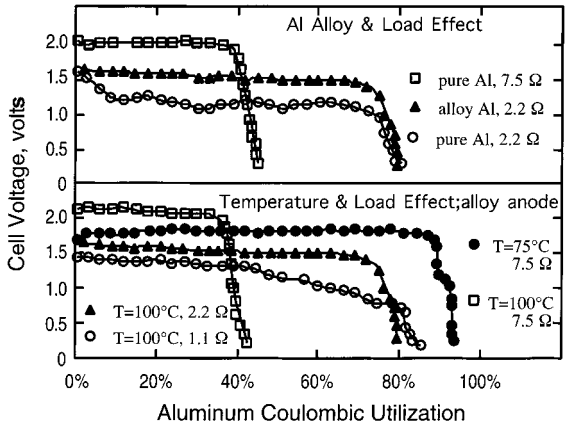

Figure 7. Cell voltage and coulombic efficiency of aluminum oxidation during discharge of aluminum/permanganate cells; effects are shown of anode composition and load (top portion), and temperature and load (bottom portion). Anodes are composed of either an ALCAN "pure" 99.999% Al or an AB50V Al "alloy" (containing less than 1% Mg, Sn, and Ga). Unless otherwise indicated, discharges are over a 2.2 Ω load at 100 °C. Electrolyte: 3 *m* KOH, 0.3 *m* $KMnO_4$. Electrolyte also contains either 0.006 *m* Na_2SnO_3 and 0.0006 *m* Ga_2O_3, for use with the indicated pure Al anode, or with only the 0.006 *m* Na_2SnO_3 for the indicated alloy anode. Further experimental conditions are described in the Figure 6 legend.

as seen in the lower portion of Figure 7, anodic utilization at 100 °C improves from up to 80% as the current density is increased from 0.5 to 2.5 A/cm^2 by using smaller load resistances. High aluminum coulombic utilization (in excess of 90%) is achieved by lowering the cell temperature to 75 °C. This lower temperature has the added advantage of stabilizing the alkaline permanganate electrolyte against decomposition, although increased polarization losses decrease the cell voltage and power density at the lower temperature.

A thin cell configuration is utilized to further enhance the specific high power attainable during aluminum/permanganate charge generation. The interelectrode gap is larger (30 μm) than that in the previous Ag/Cd example to maintain a sufficient volume to externally inject the electrolyte, triggering cell discharge. It is observed that upon discharge at 100 °C, this aluminum/permanganate cell can sustain current densities of 0.1 to over 2 A/cm^2 for 10 ms−1000 ms, depending on the applied discharge load. Within the cell, the mass of $KMnO_4$ in the 3 μL of injected electrolyte is 0.13 mg, the mass of the 1 μm film of Ni electrodeposited electrocatalyst is 0.10 mg, and the mass of consumed Al is less than 0.02 mg. In this configuration, the mass of active materials (excluding electrical contacts, solvent and enclosures) is 0.25 mg. The left hand portion of Figure 8 presents the observed aluminum/permanganate discharge characteristics. On the basis of the mass of the active cell materials (permanganate, nickel electrocatalyst, and consumed aluminum) the peak specific power measured for the cell is 0.8 MW/kg, and an average specific power of 0.6 MW/kg is sustained for 400 ms. We have found that MnO_2 buildup prevents the reuse of a single pulsed discharged cell. At a specific power of 0.4 MW/kg the cell yields 70 Wh/kg of specific energy.

As previously discussed, the cyclability of the silver/cadmium cell diminished at higher temperature. In the aluminum/permanganate cell, the electrolyte was stable at 75 °C (to within a detectability limit of 3×10^{-5} mol MnO_4^-/L min), whereas a 100 °C electrolyte undergoes moderate decomposition (8×10^4 mole/L min) as again measured with the depletion of the 526 nm MnO_4^- absorption spectral peak and rise of the 602 nm MnO_4^{2-} absorption in accordance with

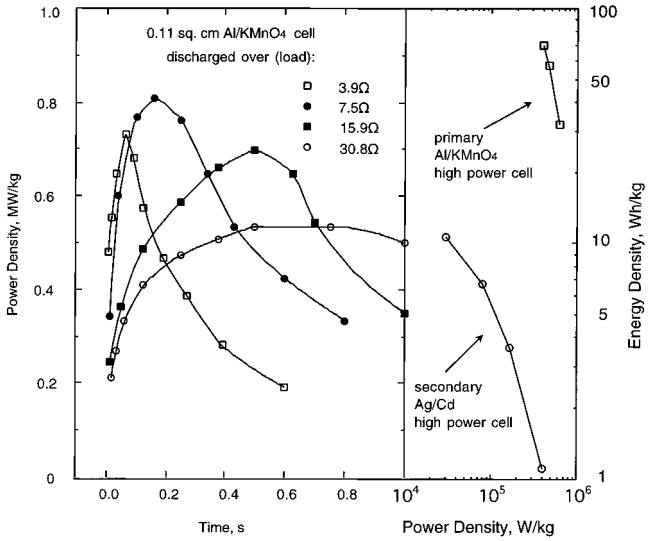

Figure 8. Left: Discharge of an aluminum/permanganate ultrahigh power cell at 100 °C showing specific power variation in time over various ±1% precision resistor discharge loads. Electrolyte: 3 *m* KOH, 0.3 *m* $KMnO_4$, 0.006 *m* Na_2SnO_4 electrolyte at 100 °C. 0.11 cm^2 anode and cathode separated by a 30 μm Teflon spacer. Anode: AB50V aluminum alloy. Separated by a 30 μm Teflon spacer from the cathode: 1 μm film of nickel electrodeposited electrocatalyst. Right: Specific power and specific energy of the electrochemical primary and secondary cell examples presented in this study and evidencing electrochemical power domains delineated in the right position of Figure 1.

$$2MnO_4^- + 2OH^- \rightarrow 2MnO_4^{2-} + {}^1/_2O_2 + H_2O \quad (13)$$

As summarized in the right-hand portion of Figure 8, both the specific power for the aluminum/permanganate and the silver/cadmium secondary examples, are within the ultrahigh specific power domain of Figure 1 and approach 10^6 W/kg. Nevertheless, demonstrations of larger cells will be a challenge which to be successful must incorporate existing submicron thin film preparation techniques including electrodeposition, e-beam deposition, and chemical vapor deposition.[25]

Both of the examples presented fulfill the conditions of ultrahigh specific power (≫10000 W/kg) over a discharge time long compared to double layer times (≫1 ms). Reports in the literature indicate that fuel cells generally exhibit low power per unit mass, although power per unit area can be high. Hence, a solid oxide electrolyte fuel cell with power density of 1.5 W/cm^2 has been reported.[25] There have been few reports in the literature of attempts to access the highest electrochemical power domains. Power bursts were demonstrated from a secondary battery (0.25 MW/kg) discharged during short duration near the double layer charging time (100 μs); overlayer formation substantially diminished the power during longer discharge times.[26] In the longer (millisecond) time domain, the only other high specific power cell we have found reported is a 0.075 MW/kg for the 400 °C discharge of a molten LiAl/FeS_2 cell although it has been suggested that inclusion of the mass of the requisite high temperature supporting materials may diminish that calculation of specific power.[27−28]

Conclusions

Compared to capacitors, studies of faradaic processes conventionally have assumed they can achieve high specific energy, of over 1 Wh/kg, but limited specific power of substantially less than 1000 W/kg. This study has probed an unusually high specific power domain for faradaic processes. The electro-

chemical ultrahigh power domain, is defined as a specific power over 10000 W/kg occurring at specific energy over 1 Wh/kg, for faradaic discharge times long compared to the electrochemical double layer charging time. Five criteria are probed which facilitate the electrochemical ultrahigh power domain: (1) kinetically facile anodic and cathodic redox couples; (2) a high activity of redox constituents relative to electrode surface area; (3) a low electrolyte resistance; (4) time domains longer than the double layer time, but short compared to the onset of mass transport limitations. The discharge time t_d is on the order of milliseconds to seconds for concentrated aqueous cells. (5) The final criteria is a low cross sectional thickness of each of the cell components compared to its mass m_i.

Experimental evidence and examples of both irreversible and quasi-reversible faradaic processes which occur in the ultrahigh power domain are presented. Both of the examples have specific powers approaching 10^6 W/kg. The irreversible example establishes electrochemical control of the chemically reactive couple aluminum and permanganate redox couples. The secondary quasi-reversible example utilizes a silver/cadmium electrochemical storage couple systematically reduced to the submicron and micron microelectrochemical cross section domain (submicron Ag and Cd electrodes separated by a 5 μm interelectrode gap).

Acknowledgment. We are grateful for support by the Israel-Japan Scientific Cooperation, the Israel Science Foundation founded by the Israel Academy, Dr. Catherine Marsh and ASEE/ONR, and the Technion's VPR Promotion of Research.

References and Notes

(1) *Energy Workshop on Advanced Battery Technology* R&D; Division of Chemical Sciences, Office of Basic Energy Science, U.S. Department of Energy: Washington, DC, 1992.

(2) Oyama, N.; Tatsuma, T.; Sato, T.; Sotomura, T. *Nature* **1995**, *373*, 598−600.

(3) Wu, L.; Dahn, J. R.; Wainwright, D. S. *Science* **1995**, *264*, 1115−1118.

(4) Armstrong, A. R.; Bruce, P. G. *Nature* **1996**, *381*, 499−502.

(5) *Proceedings of the 5th International Conference on Double Layer Capacitors and Similar Energy Storage Devices*, Florida Educational Seminars; Boca Raton, FL, 1995.

(6) *Proceedings of the Symposium on New Sealed Rechargeable Batteries and Supercapacitors* (eds Barnett, B. M., et al., Eds.; Electrochemical Society: Pennington, 1993; Vol. 93-23.

(7) Mayer, S. T.; Pekala, R. W.; Kascj, J. L. *J. Electrochem. Soc.* **1993**, *140*, 446−451.

(8) Amatore, C. In Physical Electrochemistry; Rubinstein, I., Ed., Dekker: New York, 1995; pp 131−208.

(9) Licht, S.; Cammarata, V.; Wrighton, M. S. *Science* **1989**, *243*, 1176−1178.

(10) Buck, R. P.; Nahir, T. M.; Mackel, R.; Liess, H. *J. Electrochem. Soc.* **1992**, *139*, 1611−1618.

(11) Overbeek, J. Th. G. *Electrochemistry*; Center for Advanced Engineering Study, MIT: (Cambridge, 1981, Part V (Electrode Kinetics) Catalogue 61−2300.

(12) Linden, D. Handbook of Batteries, McGraw-Hill: NY, 1984.

(13) Licht, S. *J. Electrochem. Soc.* **1997**, *144*, L133−L136.

(14) Licht, S.; Marsh, C. *J. Electrochem. Soc.* **1992**, *139*, L109−L111.

(15) Licht, S.; Jeitler, J. R.; Hwang, J. H. *J. Phys. Chem.* **1997**, *101*, 4959−4965.

(16) Licht, S.; Marsh, U.S. Patent **5,549,991**, Aug 27, 1996.

(17) Licht, S.; Peramunage, D. *Science* **1993**, *261*, 1029−1023.

(18) Macdonald, D. D.; Real, S.; Urquidi-Macdonald, M. *J. Electrochem. Soc.* **1988**, *135*, 2397.

(19) Hunter, J. Ph.D. Thesis, University of Oxford, 1989.

(20) Bohnstedt, W. *J. Power Sources* **1980**, *20*, 245.

(21) Licht, S.; Peramunage, D. *J. Electrochem. Soc.* **1993**, *140*, L4−L6.

(22) Macdonald, D. D.; English, C. *J. Appl. Electrochem.* **1990**, *20*, 405.

(23) Tarcy, G. P. U.S. Patent **4,950,560**, Aug 21, 1990.

(24) Licht, S.; Myung, N. *J. Electrochem. Soc.* **1995**, *142*, L179−L182.

(25) *Proceedings of the Coatings and Surface Modification*; Kendig, M., et al., Eds.; Electrochemical Society Pennington, 1993; Vol. 93-28.

(26) Sasaki, H.; Suzuki, M.; Otoshi, S.; Kajimura, A.; Ippommatsu, M. *J. Electrochem. Soc.* **1992**, *139*, L12−L13.

(27) LaFollette, R. M.; Bannion, D. N. *J. Electrochem. Soc.* **1990**, *137*, 3693.

(28) Gibbard, F. *Proc. Electrochem. Soc.* **1986**, *86-12*, 15.